Supplementary Information for

Synergistic Dual Sites in a Cobalt-Porphyrin Polymer Enable Tunable Syngas Production from CO_2 Photoreduction

Guangfu Zhou, Bin Chen*, Ting-Ting Li*

School of Materials Science and Chemical Engineering, Ningbo University, Ningbo, Zhejiang, 315211, China.

*Corresponding author. E-mail address: chenbin2@nbu.edu.cn (B. Chen); litingting@nbu.edu.cn. (T.-T. Li).

Experimental section

Materials

Pyrrole, 2,2'-bipyridil-5,5'-dialdehyde (Bpy), biphenyl-4,4'-dicarboxaldehyde (Bpda), 4-biphenylcarbaldehyde, anhydrous methanol (MeOH), nitrobenzene (NBZ), trifluoroacetic acid (TFA), acetic acid (HOAc), and $CoCl_2 \cdot 6H_2O$ were purchased from Macklin Co. $Ru(bpy)_3Cl_2 \cdot 6H_2O$ (98%) and DMF (99.9%) were purchased from Energy Chemical Co., Ltd. Triethanolamine (TEOA) was obtained from Aladdin Co., Ltd. All the chemicals and solvents were used directly without further purification.

Synthesis of 5,10,15,20-tetra(4-biphenyl) porphyrin

4-biphenylcarboxaldehyde (95 mg, 0.52 mmol), TFA (0.2 mL), and nitrobenzene (1.8 mL) were added to a 250 mL round-bottom flask containing glacial acetic acid (100 mL). The mixture was ultrasonicated to ensure homogeneous dispersion of the starting materials. Pyrrole (36.5 μL, 0.52 mmol) was then added dropwise, followed by further ultrasonication. The reaction mixture was heated to 80 °C and stirred under reflux for 24 h. The solvent is partially removed by reduced-pressure distillation. Methanol was added to the residue, and the mixture was kept in a refrigerator overnight. The resulting precipitate was collected by filtration, washed sequentially with water and methanol, and dried to afford 5,10,15,20-tetra(4-biphenyl) porphyrin. ^{1}H NMR (500 MHz, chloroform-*d*) δ 8.97 (s, 8H), 8.32 (d, *J* = 7.7 Hz, 8H), 8.02 (d, *J* = 7.5 Hz, 8H), 7.95 (d, *J* = 7.6 Hz, 8H), 7.61 (t, *J* = 7.8 Hz, 8H), 7.49 (t, *J* = 8.5 Hz, 4H), -2.69 (s, 2H).

Synthesis of BpyPOP

Bpy (55.2 mg, 0.26 mmol) was added to a 250 mL round-bottom flask with 100 mL acetic acid and sonicated for 10 min. Then NBZ (1.8 mL), TFA (0.2 mL) were added to the aforementioned solution to act as the catalyst and oxidant, respectively. After that, pyrrole (36.5 μL, 0.52 mmol) was subsequently added dropwise to the aforementioned solution, and the mixture was subjected to continued ultrasonication for 30 min. The resulting mixture was kept at 80 °C and stirred continuously for 24 h. After cooling to room temperature，the black product was collected by filtration and

washed with deionized water and ethanol to remove the solvent and unreacted raw materials. Afterward, black product was finally obtained after vacuum drying at 60 °C for 24 h.

The synthesis of BpdaPOP and Sp-CoBpyPOP followed the protocol established for BpyPOP, with the sole modification being the replacement of the Bpy with Bpda or [Co(Bpy)Cl_2], respectively.

Synthesis of CoBpyPOP

The catalyst precursor BpyPOP (50 mg) was added into a 15 mL DMF in a round-bottom flask and sonicated for 30 min. The mixture was then placed in an oil bath and heated to 100 °C. Subsequently, $CoCl_2 \cdot 6H_2O$ (140 mg) was introduced into the system. The temperature was raised to 160 °C, and the reaction was allowed to proceed under continuous stirring for 6 h. After cooling to room temperature, the black product was collected by filtration and washed with deionized water and ethanol to remove the solvent and $CoCl_2 \cdot 6H_2O$ that did not coordinate with BpyPOP.

The synthesis of CoBpdaPOP followed protocol established for CoBpyPOP.

Synthesis of Co(Bpy)Cl_2

$CoCl_2 \cdot 6H_2O$ (61.8 mg, 0.26 mmol) and Bpy (55.2 mg, 0.26 mmol) were uniformly dissolved in anhydrous methanol (10 mL) in a Beaker. It was then stirred at room temperature for 12 h. After reaction, dark green microcrystals were formed as the solvent slowly evaporated at room temperature. The crude product was collected and washed with cold anhydrous ethanol (3 × 5 mL) by vacuum filtration to remove unreacted starting materials. Finally, the solid was dried under vacuum at 60 °C for 24 h to yield Co(Bpy)Cl_2 as a dark green crystalline powder.

Characterizations

The morphology of the samples was obtained using a field emission scanning electron microscope (SEM, Hitachi S-4800 II) and a FEI Tecnai G2 F20 electron microscope. EDS analysis was carried out on a FEI Tecnai G2 F20 electron microscope equipped with a fitted with an elemental mapping and energy dispersive spectroscopy (EDS). Powder X-ray diffraction (PXRD) patterns of the powder samples were

obtained with a Bruker D8 Advanced diffractometer with Cu Kα radiation at 40 kV and 40 mA. Fourier transform infrared (FT-IR) spectroscopy information was obtained by a Thermo Scientific Nicolet iS20 FT-IR spectrometer. X-ray photoelectron spectroscopy (XPS) was performed with a Thermo Scientific K-Alpha XPS system. Inductively coupled plasma optical emission spectroscopy (ICP-OES) was performed with a Thermo Fisher iCAP PRO to obtain the Co content in the materials. The Brunauer-Emmett-Teller (BET) surface area and porous structure were determined by N_2 sorption with an Accelerated Surface Area and Porosimetry 2020 (ASAP 2020) adsorption apparatus. CO_2 sorption was performed with ASAP 2020 adsorption apparatus. The solid UV-Vis diffuse reflectance spectra were measured by a UV-Vis spectrophotometer (SHIMADZU) from 250 to 800 nm and $BaSO_4$ was used as the reflectance standard. Furthermore, The X-ray absorption fine structure (XAFS) spectra at the Co K-edge were collected using an easyXAFS300+ system (easyXAFS LLC) equipped with a Mo X-ray tube, a silicon drift detector (KETEK AXAS-M2), and spherically bent crystal analyzers (SBCA) arranged in Rowland geometry. The gaseous products were analyzed using a gas chromatograph equipped with both a thermal conductivity detector (TCD) and a flame-ionization detector (FID) coupled with a methanizer.

Electrochemical measurements

All electrochemical measurements were performed with a CHI760D workstation in a conventional three-electrode cell, using the catalyst-modified ITO (geometric area 1 cm^2) as the working electrode, a Pt plate as the counter electrode, and an Ag/AgCl (saturated KCl) reference electrode. The working electrode was fabricated by dispersing 4 mg of the as-synthesized powder in 500 μL isopropanol containing 20 μL of 5 wt % Nafion solution under sonication for 30 min to obtain a homogeneous catalyst ink. An aliquot of the ink (80 μL cm^{-2}) was then drop-casted onto an ITO-coated glass substrate (geometric area = 1 cm^2) and dried under ambient conditions. Electrochemical impedance spectroscopy (EIS) was performed in the aqueous solution of 2 M Na_2SO_4 in the range of 0.01 Hz to 100 kHz. Mott-Schottky analyses was performed in 2 M

Na_2SO_4 at frequencies of 500, 1000, and 1500 Hz under potentiostatic control.

Photocatalytic Experiments

Photocatalytic CO_2 reduction experiments were conducted in a custom quartz photoreactor with the internal volume of 60 mL. In a typical photocatalytic experiment, 2.0 mg of catalyst and 10.0 mg of $Ru(bpy)_3Cl_2 \cdot 6H_2O$ ([Ru]) were dispersed in 20 mL of mixed solvent (CH_3CN:H_2O:TEOA = 3:1:1, v/v/v), then the custom quartz photoreactor was purged with pure CO_2 gas for 10 min to displace air, and then sealed. Then a 10 W LED lamp was used as the light source. During the reaction, the temperature of the reaction solution was kept at 25 °C. The generated gaseous and liquid products were detected and quantified by gas chromatography (GC) and ^1H nuclear magnetic resonance (^1H NMR) spectroscopy, respctively.

In situ diffuse reflectance infrared Fourier transform spectroscopy (DRIFTS)

In situ DRIFTS measurements were performed with a Thermo Scientific Nicolet iS50 spectrometer equipped with a mercury cadmium telluride (MCT) detector. Firstly, a semi-cylindrical silicon ATR crystal was sequentially polished with alumina and silica suspensions to achieve a hydrophobic surface prior to use. A thin Au layer was chemically deposited onto the crystal surface, serving as an infrared signal amplifier. The catalyst ink was prepared and uniformly deposited onto the Au-coated surface. The sample compartment was loaded with the $[Ru(bpy)_3]Cl_2$ solution prepared in TEOA/MeCN/H_2O mixture and subsequently purged with CO_2 to simulate the photocatalytic reaction environment. After 20 min, the specimen chamber-loaded sample was irradiated with a 300 W xenon lamp, and Infrared absorption spectra were collected at 5-minute intervals in real-time.

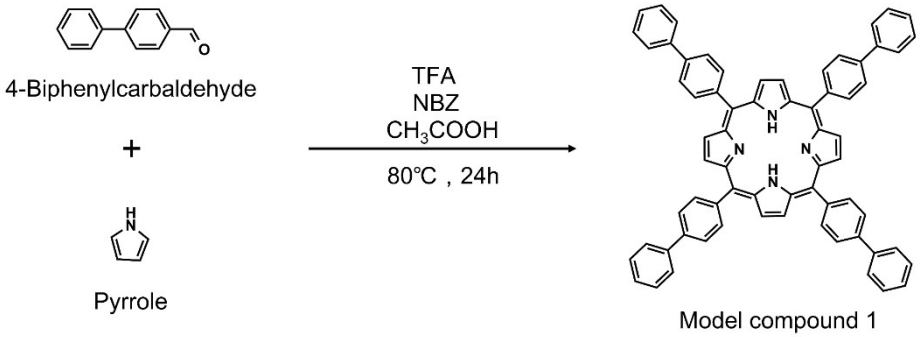

Fig. S1. Synthesis of model compound 1 5,10,15,20-tetra(4-biphenyl) porphyrin from pyrrole and 4-biphenylcarbaldehyde.

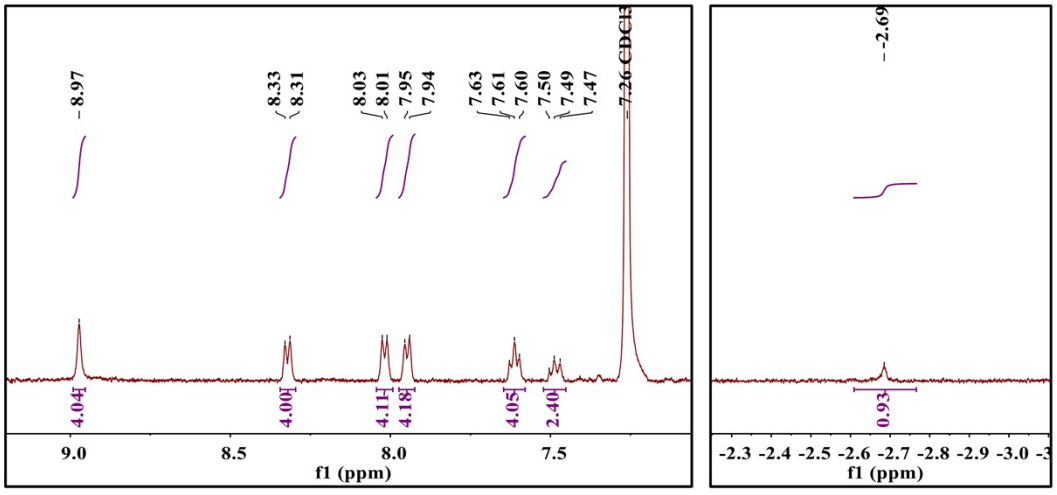

Fig. S2. ^{1}H NMR spectrum of 5,10,15,20-tetra(4-biphenyl) porphyrin.

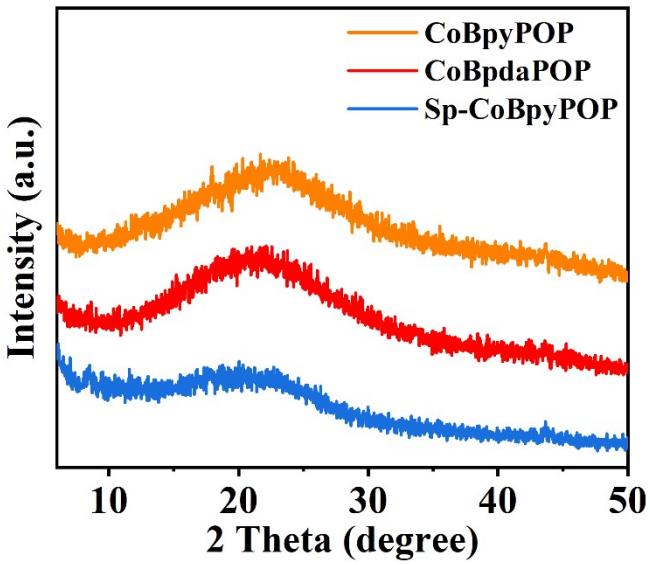

Fig. S3. The PXRD patterns of CoBpyPOP, CoBpdaPOP, and Sp-CoBpyPOP.

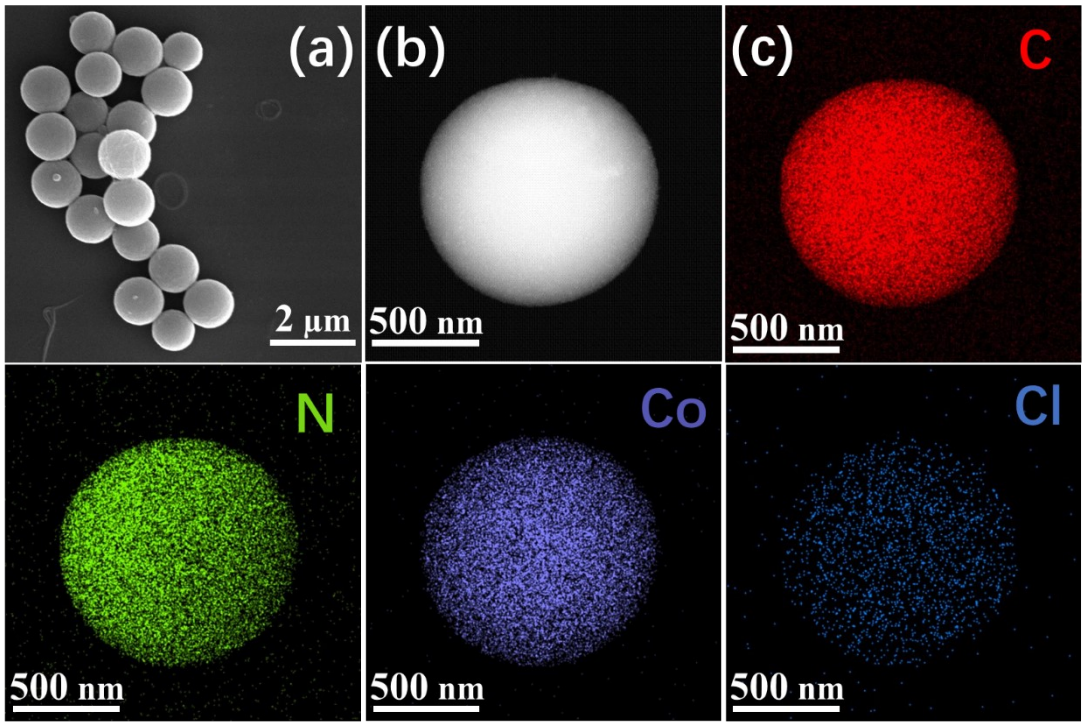

Fig. S4. (a) SEM and (b) TEM images of CoBpyPOP; (c) Elemental mapping of CoBpyPOP.

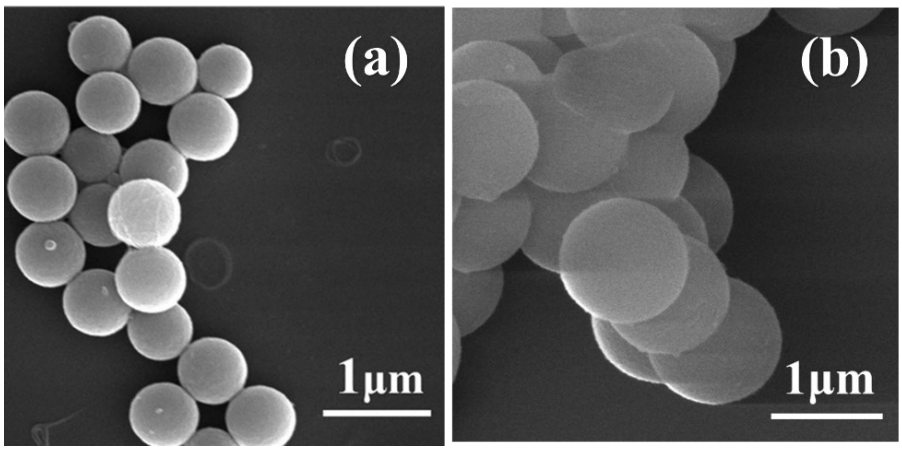

Fig. S5. The SEM images of (a) Sp-CoBpyPOP and (b) CoBpdaPOP.

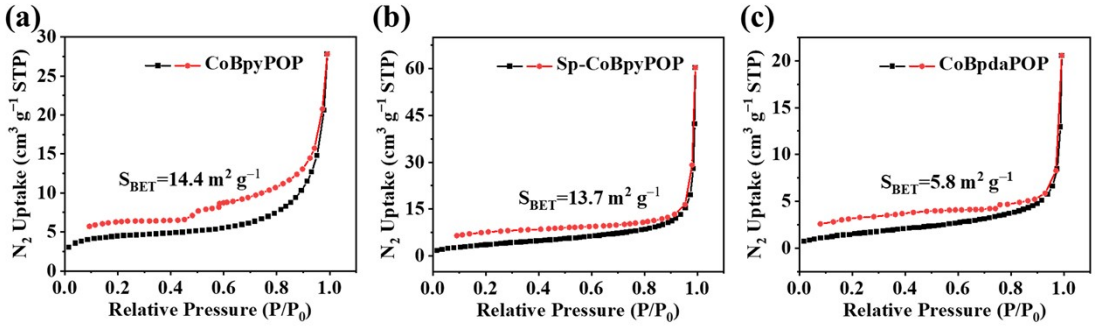

Fig. S6. The N_2 sorption isotherms of CoBpyPOP, CoBpdaPOP, and Sp-CoBpyPOP at 77 K.

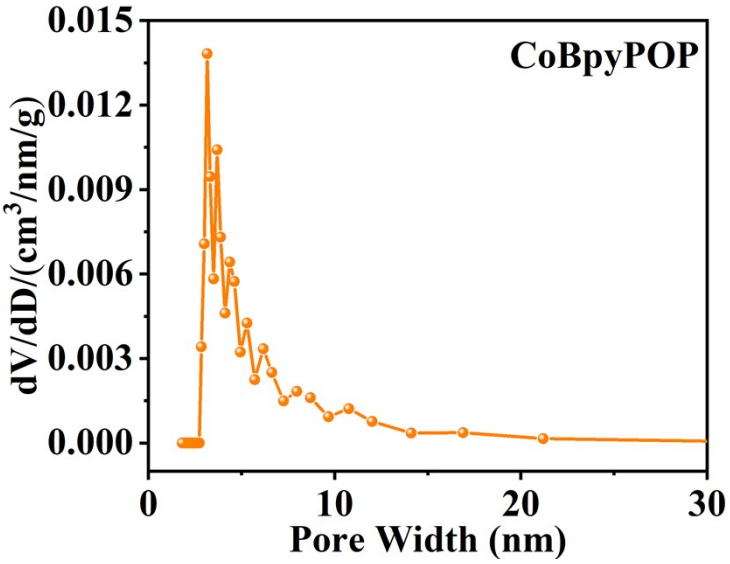

Fig. S7. Pore size distribution of CoBpyPOP.

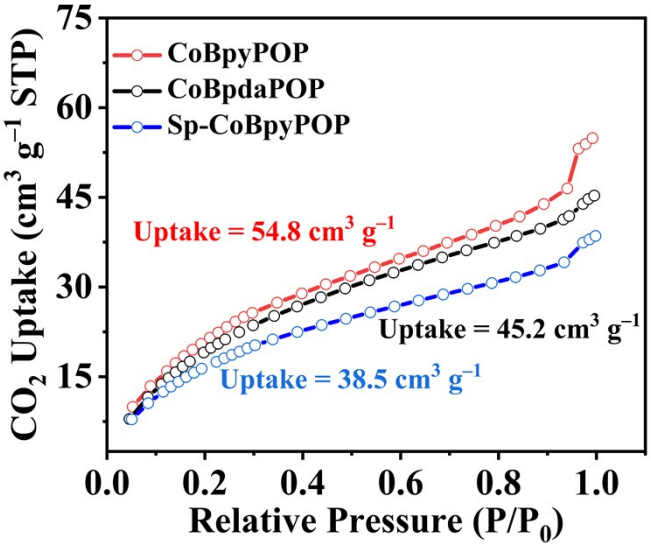

Fig. S8. The CO_2 adsorption isotherms of CoBpyPOP, CoBpdaPOP, and Sp-CoBpyPOP at 273 K.

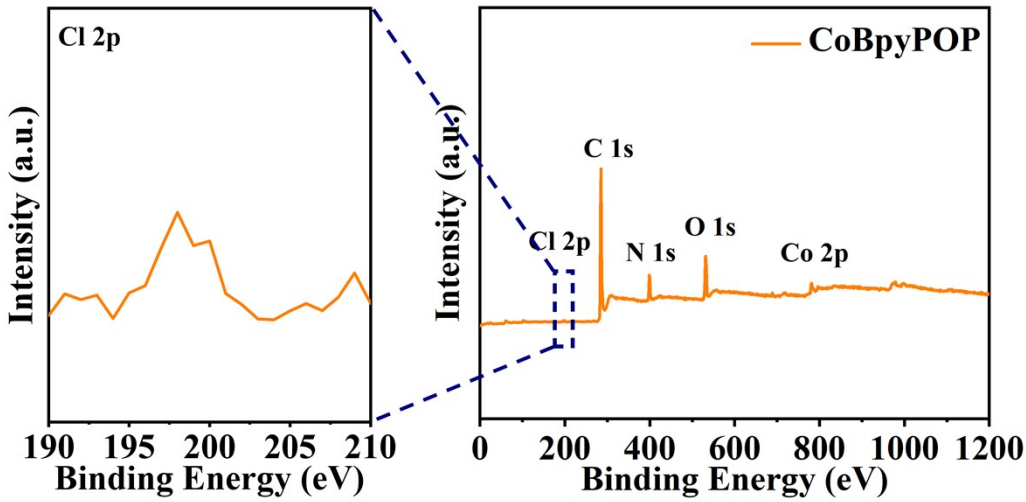

Fig. S9. XPS survey spectrum of CoBpyPOP.

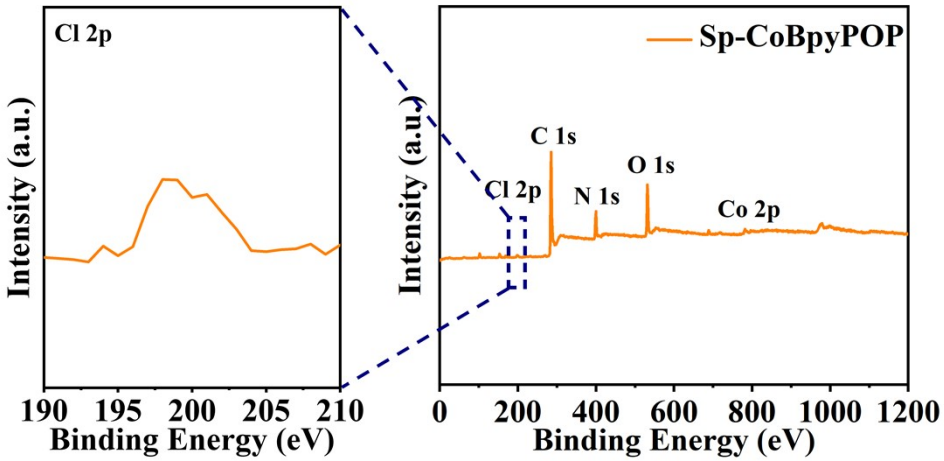

Fig. S10. XPS survey spectrum of Sp-CoBpyPOP.

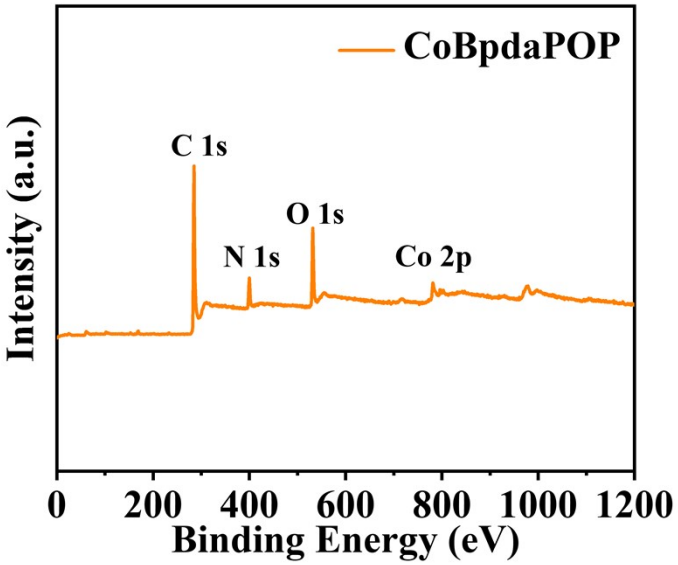

Fig. S11. XPS survey spectrum of CoBpdaPOP.

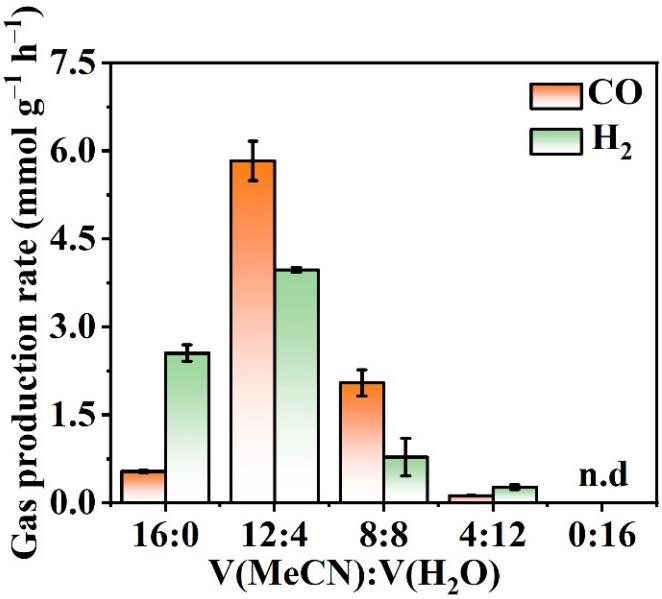

Fig. S12. Photocatalytic performance of CoBpyPOP in the CO_2-saturated MeCN/H_2O mixture with different MeCN/H_2O ratios.

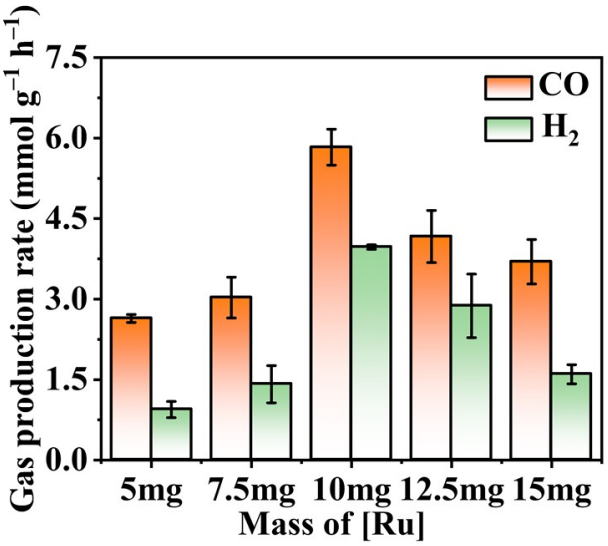

Fig. S13. Photocatalytic performance of CoBpyPOP in the CO_2-saturated MeCN/H_2O mixture with the addition of various mass of [Ru].

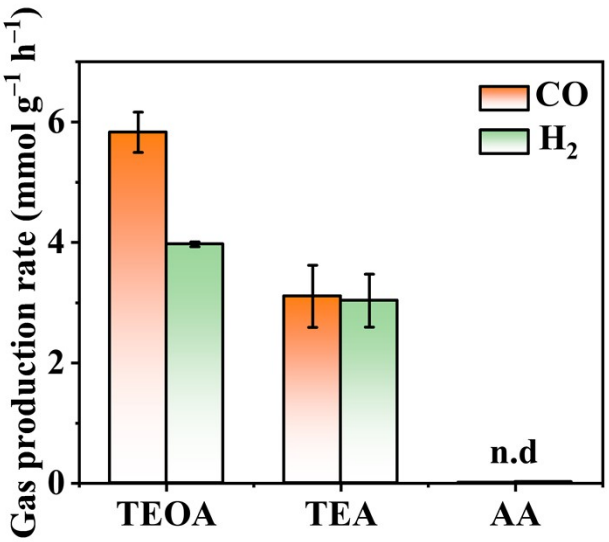

Fig. S14. Photocatalytic performance of CoBpyPOP in the CO_2-saturated MeCN/H_2O mixture with the addition of different sacrificial agent (triethanolamine: TEOA; triethylamine: TEA; ascorbic acid: AA).

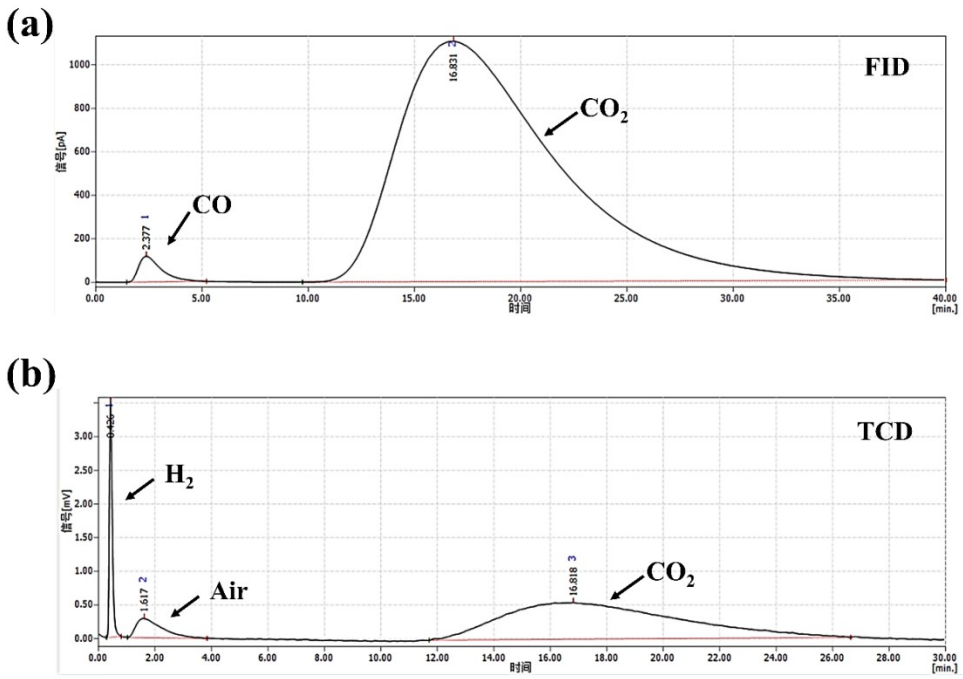

Fig. S15. Gas chromatography analysis for the gas products.

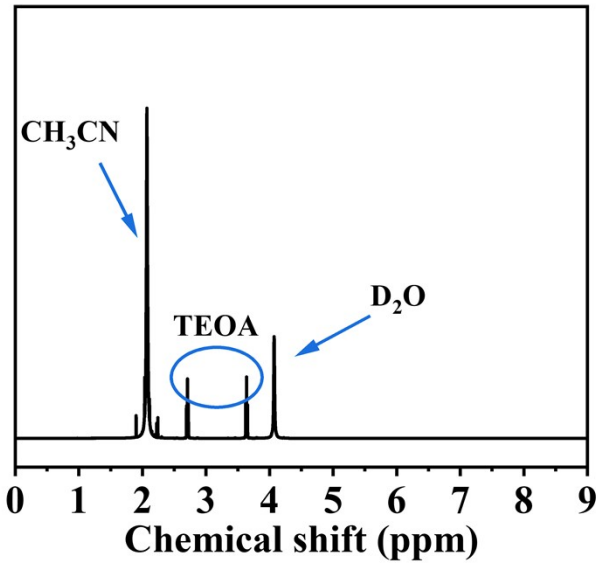

Fig. S16. ^1H NMR spectrum of the liquid phase from the reaction system after photocatalytic CO_2 reduction. Reaction conditions: CoBpyPOP (2 mg), [Ru] (10 mg), MeCN (12 mL), H_2O (4 mL), TEOA (4 mL), CO_2 (1 atm) and visible light-irradiation ($\lambda \geq 420$ nm), room temperature, 2 h.

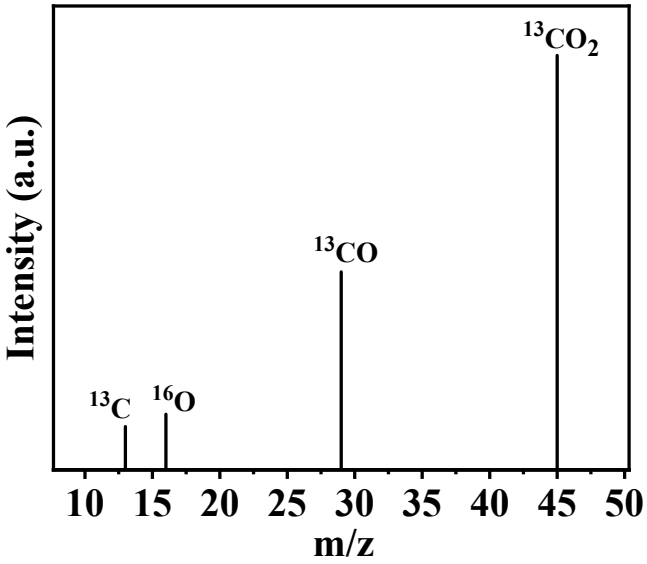

Fig. S17. Mass spectrum of the gaseous product obtained from the photocatalytic CO_2 reduction over CoBpyPOP in MeCN /H_2O/TEOA (v:v:v = 3:1:1) using $^{13}CO_2$ instead of $^{12}CO_2$.

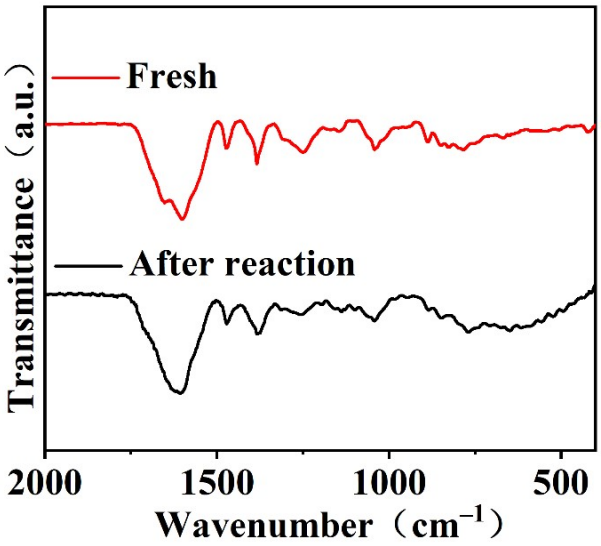

Fig. S18. The comparison of FT-IR spectra of CoBpyPOP before and after stability test.

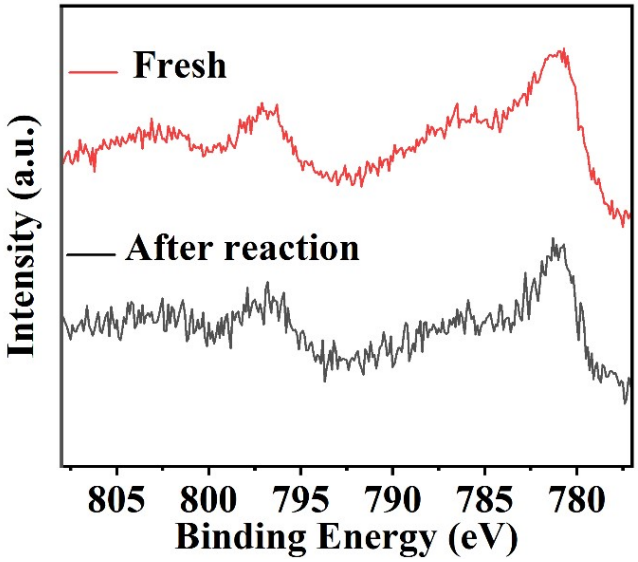

Fig. S19. The comparison of Co 2p XPS spectra of CoBpyPOP before and after stability test.

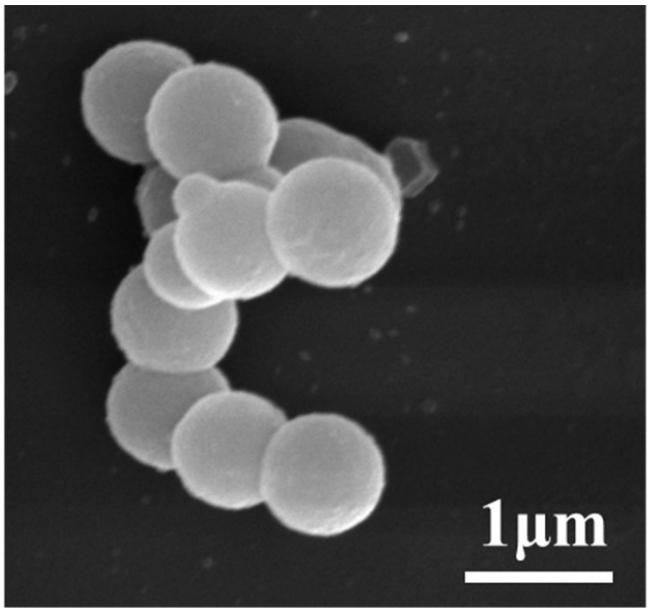

Fig. S20. The SEM image of CoBpyPOP after stability test.

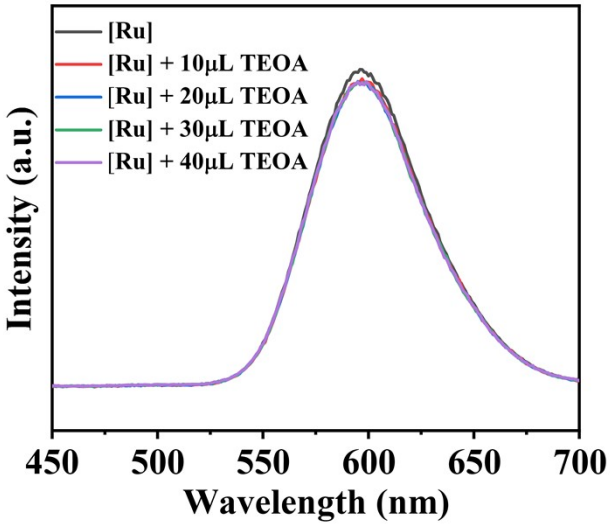

Fig. S21. Steady-state photoluminescence spectra of a MeCN/H_2O mixture of [Ru] with the addition of different volumes of TEOA.

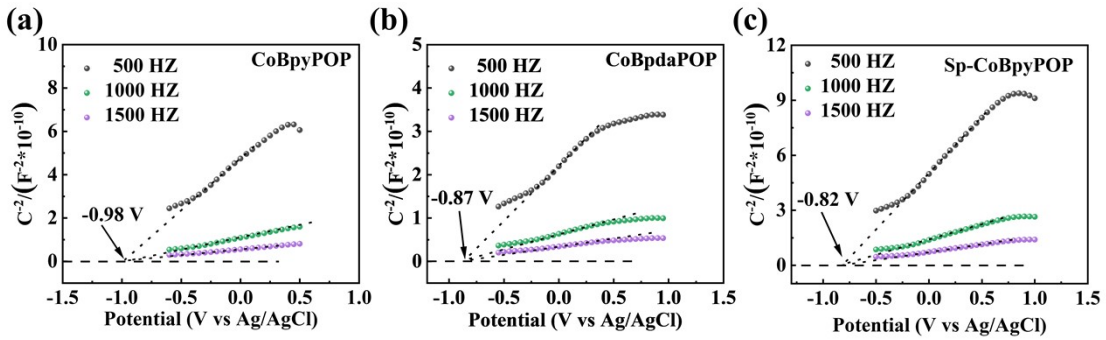

Fig. S22. Mott-Schottky plots of (a) CoBpyPOP, (b) CoBpdaPOP, and (c) Sp-CoBpyPOP.

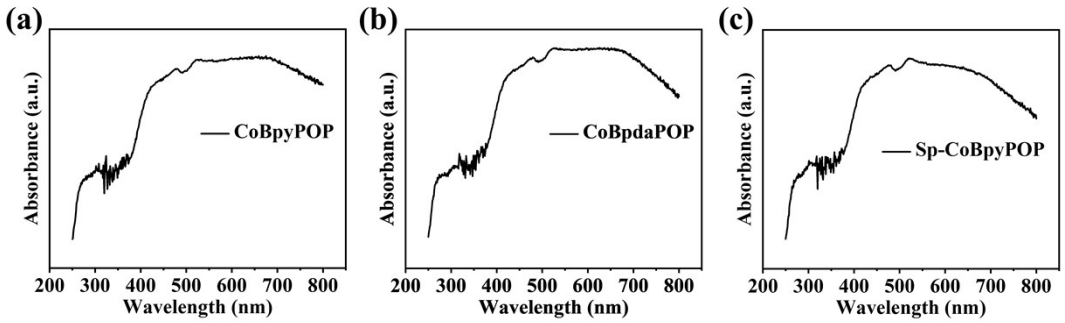

Fig. S23. UV-Vis DRS spectra of (a) CoBpyPOP, (b) CoBpdaPOP, and (c) Sp-CoBpyPOP.

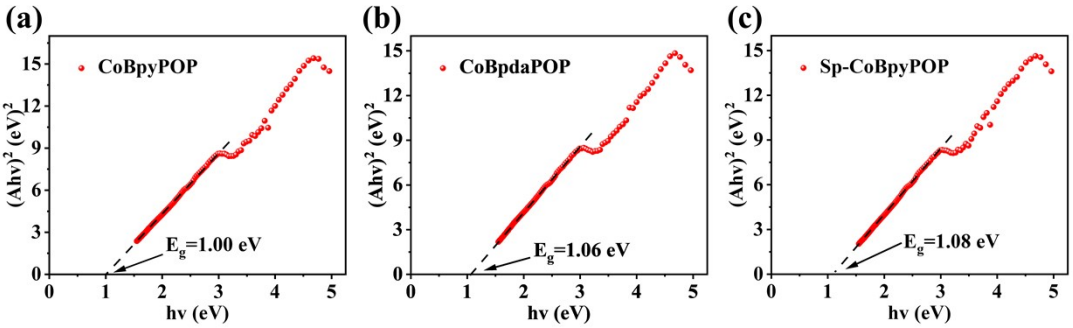

Fig. S24. Tauc plots of (a) CoBpyPOP, (b) CoBpdaPOP, and (c) Sp-CoBpyPOP.

Table S1. The Co contents in the samples (based on ICP-OES results).

Samples	Co (wt%)
CoBpyPOP	7.4
Sp-CoBpyPOP	3.4
CoBpdaPOP	2.7

Table S2. Co K-edge EXAFS curve fitting parameters.

Sample	Path	CN	R (Å)	σ^2 (10^{-3} Å^2)	R factor
Co foil	Co-Co	12	2.49	5.8	0.001
CoBpyPOP	Co-N	3.1	1.92	9.5	0.005
	Co-Cl	1.9	2.26	9.5	0.005

CN is the coordination number; R is interatomic distance; σ^2 is Debye-Waller factor (a measure of thermal and static disorder in absorber-scatterer distances); R factor is used to value the goodness of the fitting.

Table S3. The comparison of photocatalytic CO_2 reduction performance towards syngas production with other reported organic frameworks-based photocatalysts.

Photocatalyst	Photosensitizers/Sacrificial agent	Reaction solvent	CO production rate (mmol $g^{-1}h^{-1}$)	H_2 production rate (mmol $g^{-1}h^{-1}$)	Syngas production rate (mmol $g^{-1}h^{-1}$)	n(CO) /n(H_2)	Ref.
CoBpyPOP	[Ru]/TEOA	CH_3CN/H_2O	5.8	4.0	9.8	1.4:1	This work
POP2-Fe	[Ru]/TEOA	DMF/H_2O	3.04	3.75	6.79	0.8:1	[1]
Co@COF-TVBT-Bpy	[Ru]/TEOA	CH_3CN/H_2O	1.13	1.16	2.29	1:1	[2]
NiPc-CoPOP	[Ru]/TEOA	CH_3CN/H_2O	4.27	3.64	7.91	1.2:1	[3]
ImI-CMP@Co	[Ru]/TEOA	CH_3CN/H_2O	2.95	5.90	8.85	0.5:1	[4]
Co-CMP-qaDA	[Ru]/TEOA	CH_3CN/H_2O	5.28	7.92	13.2	0.7:1	[5]
CoPor-DPP-COF	[Ru]/TIPA	CH_3CN/H_2O	10.20	2.24	12.44	4.6:1	[6]
Co-Por-BDT	$Re(bpy)(CO)_3Cl$/TEOA	CH_3CN	1.42	0.09	1.52	15.8:1	[7]
Co-TAPT-COF-1	[Ru]/TEOA	CH_3CN/H_2O	8.39	11.31	19.70	0.7:1	[8]
Co-TAPT-COF-2	[Ru]/TEOA	CH_3CN/H_2O	3.50	4.72	8.22	0.7:1	
O_1S_3–Ni COPs	[Ru]/TEOA	CH_3CN/H_2O	4.18	4.26	8.44	1:1	[9]
DA-CTF@DPT-Co	TEOA	CH_3CN/H_2O	0.69	0.72	1.41	1:1	[10]

[Ru]: $Ru(bpy)_3Cl_2$, TEOA: triethanolamine, TIPA: triisopropanolamine.

References:

1 X. Yao, K. Chen, L.-Q. Qiu, Z.-W. Yang and L.-N. He, *Chem. Mater.*, 2021, **33**, 8863–8872.

2 J.-X. Cui, Y.-M. Fu, B. Meng, J. Zhou, Z.-Y. Zhou, S.-M. Liu and Z.-M. Su, *J. Mater. Chem. A*, 2022, **10**, 13418–13427.

3 X. Dong, Y. Si, Q. Wang, S. Wang and S. Zang, *Adv. Mater.*, 2021, **33**, 2101568.

4 W. Zhao, D. Zhai, C. Liu, D. Zheng, H. Wu, L. Sun, Z. Li, T. Yu, W. Zhou, X. Fang, S. Zhai, K. Han, Z. He and W. Deng, *Appl. Catal. B Environ.*, 2022, **300**, 120719.

5 F. Wen, L. Song, X. Lv, S. Wang, G. Zheng and Q. Han, *Appl. Catal. B Environ. Energy*, 2025, **365**, 124929.

6 X. Wang, X. Ding, T. Wang, K. Wang, Y. Jin, Y. Han, P. Zhang, N. Li, H. Wang and J. Jiang, *ACS Appl. Mater. Interfaces*, 2022, **14**, 41122–41130.

7 Y. H. Kim, J. Jeon, Y. Kim, H. Noh, J. Seo, J. Kim, G. Lee and J. Baek, *Angew. Chem. Int. Ed.*, 2023, **62**, e202307991.

8 W. Zhou, X. Wang, W. Zhao, N. Lu, D. Cong, Z. Li, P. Han, G. Ren, L. Sun, C. Liu and W.-Q. Deng, *Nat. Commun.*, 2023, **14**, 6971.

9 P. Li, W. Chen, Y. Yang and J. Shen, *ACS Appl. Mater. Interfaces*, 2023, **15**, 40519–40528.

10 K. Kong, H. Zhong, F. Zhang, H. Lv, X. Li and R. Wang, *Adv. Funct. Mater.*, 2025, **35**, 2417109.